Jour. of the KGS, Vol. 23, No. 9. September 2007, pp. 17~28

# Prediction of Deformation Behavior of a Shallow NATM Tunnel by Strain Softening Analysis

## 연화모델을 이용한 저토피 NATM 터널의 변형거동의 예측

Lee, Jae-Ho[1] 이 재 호
Akutagawa, Shinich[2] 아쿠타가와 신니치
Kim, Young-Su[3] 김 영 수

## 요 지

도심지 지하 터널은 주변 구조물의 존재 하에서 미고결성 저토피고 지반에 건설되는 경우가 많기 때문에 일반 산악 터널이나 대심도 암반층에 건설되는 지하공동과는 달리 터널 주변의 지반 변위, 지표면 침하와 기울기가 터널 설계의 주요인자가 된다. 본 논문은 도심지 NATM 터널의 변형거동에 대한 합리적 해석 방법의 확립을 위한 연구로서 변형률 연화 모델을 이용한 수치해석적인 방법을 통하여 굴착에 따른 지반 평가와 거동 예측을 수행하였다. 적용되어진 변형률 연화모델은 지반이 항복후 전단변형률의 증가에 따른 전단강성와 강도정수의 저하를 고려한 것이다. 현장 계측 결과는 시공중 설계물성치의 재설정에 이용되어졌다. 연화모델의 결과와 현장 계측값과의 비교에서 적용되어진 모델이 지표 침하, 기울기, 지중 침하 및 지중 수평변위의 변형 양상을 어느 정도 재현될 수 있음을 알 수 있었다. 본 논문에서 제안된 모델을 토대로 시공조건이 엄밀한 도심지 터널의 변형거동에 정량적인 평가 및 예측이 가능할 것으로 기대된다.

## Abstract

Urban tunnels are usually important in terms of prediction and control of surface settlement, gradient and ground displacement. This paper has studied the application of strain softening analysis to predict deformation behavior of an urban NATM tunnel. The applied strain softening model considered the reduction of shear stiffness and strength parameter after yielding with strain softening effects of a given material. Measurements of surface subsidence and ground displacement were adopted to monitor the ground behavior resulting from the tunneling and to modify tunnel design. The numerical analysis results produced a strain distribution, deformational mechanism and surface settlement profile, which are in good agreement with the results of case study. The approach of strain softening modeling is expected to be a good prediction method on the ground displacement associated with NATM tunneling at shallow depth and soft ground.

**Keywords** : Deformation behavior, NATM tunnel, Prediction method, Strain softening analysis

1 Member, Post-Doctoral Researcher, Dept. of Civil Engrg., Kyungpook National Univ., hero_ljh@hotmail.com, Corresponding Author
2 Associate Prof., Dept. of Architecture and Civil Engrg., Kobe Univ., Japan
3 Member, Prof., Dept. of Civil Engrg., Kyungpook National Univ.

## 1. Introduction

Currently an increasing number of urban tunnels with small overburden are excavated according to the principle of the New Austrian Tunneling Method (NATM). Urban shallow tunnels are usually important in terms of prediction and control of surface settlement, gradient and ground displacement. In recent years, numerical methods for design purpose are often used to predict deformational behavior around tunnels (Adachi et al., 1985; Wong and Kaiser, 1987; Sakurai and Akayuli, 1998; Sterpi, 1999; Gioda and Locatelli, 1999; Matsumoto, 2000; Shahin et al., 2004).

Finite element procedures have been applied not only to the ground movement prediction but also to the whole tunnel design problem, which includes simulation of the construction method, analysis of the extent and development of failed zones, design of the support system, and effects on nearby tunnels, etc. Negro and de Queiroz (2000) represented the prediction and performance on the review of numerical analysis for shallow tunnels. These papers have showed that most of the current modeling tools adopt the two dimensional finite element analysis, and the 19% of the adopted stress-strain models are given by linear elastic model and 72% employs elastic-plastic model approach. They have explained that it was still difficult under the present state of the art to predict deterministically the behavior of the ground and tunnel system in the planning and designing state, thereby resulting in an extensive difference between the predicted values and the actual behavior after excavation.

This paper has studied the application of new computational modeling to predict and identify deformation behavior of urban NATM tunnels. The proposed numerical procedure considered the reduction of shear stiffness and strength parameter after yielding with strain softening effects of a given material. A shallow tunnel in unconsolidated soil layer is currently under construction with NATM in many countries. The surface above the tunnel is mainly used for agricultural and housing land; therefore, the tunnel will pass beneath the public facilities such as roads, railways, and water channels for agriculture. Hence, measurements of surface subsidence and ground displacement were adopted to monitor the ground behavior resulting from the tunneling.

Numerical simulation, firstly, is performed with material property values, Young's modulus, $E$, Poison's ratio, $\nu$, cohesion, $c$, and friction angle, $\phi$, obtained from laboratory and field tests with 9 cases of strain softening parameters. It showed that, in initial construction stages, the measured displacements are smaller than the predicted ones in design stages. On construction, a series of parameter tuning is performed for better agreement between computed and measured quantities at the top heading excavation before the bench excavation. The identified parameters at the top heading excavation were then used to predict displacements at the final stage.

## 2. Deformation Behavior in Shallow Tunnels

Deformational behavior around a shallow tunnel is often characterized by formation of shear bands developing from tunnel shoulder reaching, sometimes, to the ground surface. Fig. 1 shows a strain distribution derived from the results of displacement measurements taken from a subway tunnel in Washington D.C (Hansmire and Cording, 1985). It is observed that the shear bands develop from the tunnel shoulder to surface ground, as a typical deformation mechanism of a shallow tunnel in a sandy ground. From Fig. 1, one possible explanation of this deformational behavior may be best stated with a help of an illustration given in Fig. 2. Region-A, surrounded by slip plane $k$-$k$, is regarded as a potentially unstable zone that may displace downward at the lack of frictional support along $k$-$k$ planes. What is separating Region-A from the surrounding is shear band $a$ formed along $k$-$k$ line with some thickness, as Region-A slides downward. The adjacent Region-B follows the movement of Region-A, leading to the formation of another shear band $b$. The direction of shear band $b$ is related to $45°+\phi/2$ ($\phi$: friction angle) and often coincides with what is called a boundary line of zone influenced by excavation. Regions -A and B correspond to the primary and secondary zones of deformational behavior pointed out earlier by Mu-

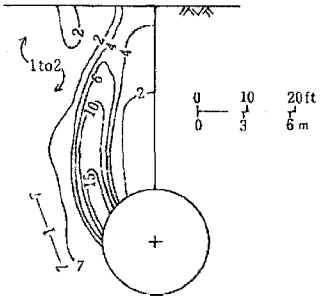


Fig. 1. Strain distribution around a subway tunnel

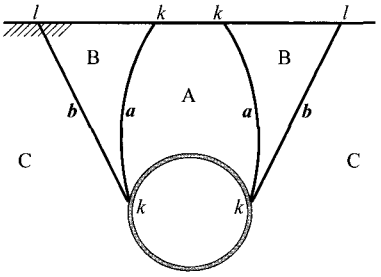


Fig. 2. Deformational mechanism in a shallow tunnel

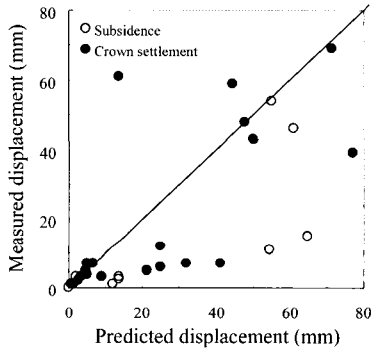


Fig. 3. Measured versus predicted displacements

rayama et al. (1969) in the series of trap door experiments. Confirming the presence of these zones is equivalent to acknowledging formation of shear bands *a* and *b*, which may not be a desirable practice in view of minimizing deformation during construction of shallow tunnels. However, it is regarded very important that a reliable method be established in order to reveal non-linear deformational mechanism and identify the state of deformation with reference to an ultimate state, which is of current interest in the new design practice. Fig. 3 shows measured displacements (surface subsidence and crown settlements) plotted against predicted ones for several tunnels with shallow overburden (Matsunaga et al., 2002).

It is recognized that in most cases the measured ones are smaller than the predicted values in design stages. This is an indication that design parameters are chosen in such a way that safety and stability of tunnels during construction be assured. However, in some cases, tunnel design could be very safe when uncertainties arise in setting up key parameters used in the design, largely due to a complicated nonlinear deformational mechanism identified around shallow tunnels.

## 3. Outline of Strain Softening Analysis

In the framework of applying general numerical analysis tools, such as finite element method, there have been series of approaches taken for simulation of tunnel excavation. Adachi et al. (1985) made use of classical slip line theory to define geometrical distribution of joint elements for modeling shallow tunnel excavation. Okuda et al. (1999) applied a back analysis procedure to identify the deformational mechanism, in which anisotropic damage parameter *m* was employed. Sterpi (1999) conducted strain softening analysis in which strength parameters (cohesion and friction angle) were lowered immediately after the initiation of plastic yielding. This approach was applied for the interpretation of field measurements by Gioda and Locatelli (1999) who succeeded in simulating the actual excavation procedure with accuracy.

These attempts incorporate some of the key factors that must be taken into consideration for modeling shallow tunnel excavation. However, there still is shortage in modeling capability, which is a primary and secondary zone in Fig. 2 to cope with development of shear bands in shallow tunneling. Matsumoto (2000) and Akutagawa et al. (2001) showed the shear band developing with excavation procedure by strain softening model and its results compared with tunnel model test. The proposed model incorporates the reduction of shear stiffness, *m* (=*E*/*G*), as well as strain softening effects of strength parameters *c* and $\phi$.

Following is a brief summary on the reduction of shear stiffness, *m* (=*E*/*G*). The x' direction coincides with the slip plane while the y' is the plane of symmetry and is

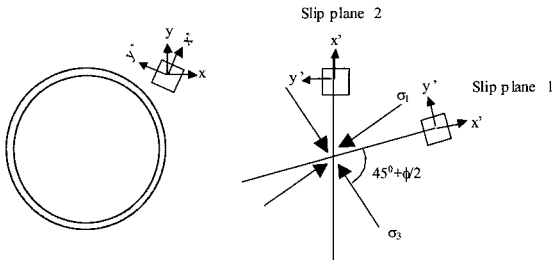


Fig. 4. Two global and local coordinate system defined for conjugate slip planes

perpendicular to the plane of isotropy. A fundamental constitutive relation between stress, $\sigma$', and strain, $\varepsilon$', is defined by Equations (1) and (2) in a local coordinate system shown in Fig. 4 (Akutagawa et al., 2006).

$$[\sigma']=[D'][\varepsilon'] \tag{1}$$

$$D'=\frac{E}{1-\nu-2\nu^2}\begin{bmatrix}1-\nu & \nu & 0\\ \nu & 1-\nu & 0\\ 0 & 0 & m(1-\nu-2\nu^2)\end{bmatrix} \tag{2}$$

An anisotropic parameter m is defined to be the ratio of $G$ to $E$ and expressed as, $m=E/G$. Therefore, we can define the damage parameter $d$ as follows:

$$m=\frac{1}{2(1+\nu)}-d \tag{3}$$

where Poisson ratio, $\nu$, is assumed to be constant. The damage parameter, $d$, can be expressed as a function of the shear strain along the slip plan as follow:

$$d=(m_e-m_r)[1-\exp\{-100\alpha(\gamma-\gamma_e)\}] \tag{4}$$

where $m_e$ is the initial value of $m$, $m_r$ is the residual value, $\alpha$ is a constant, $\gamma$ is shear strain, $\gamma_e$ is the shear strain at the onset of yielding. However, $m$ is lowered immediately after the initiation of plastic yielding (Sakurai and Akayuli, 1998). The constitutive relationship is defined for conjugate slip plane direction ($45° \pm \phi/2$) and transformed back to the global coordinate system. Equation (2) can be transformed to global coordinates as follows:

$$[D]=[T][D'][T]^T \tag{5}$$

where, $[T]$ is a transformation matrix. The stress strain

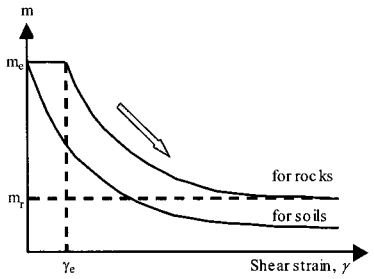


(a) Reduction of shear stiffness, $m$

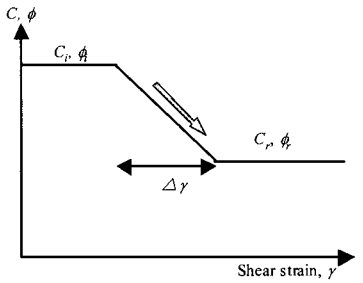


(b) Strain softening effect of strength parameter

Fig. 5. Concept of strain softening modeling

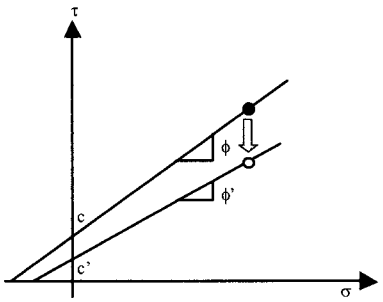


Fig. 6. Modified stress state by cohesion reduction

relationship for the global coordinate system is given in the following form:

$$[\sigma]=[D][\varepsilon] \tag{6}$$

$$D=\frac{E}{1-\nu-2\nu^2}\begin{bmatrix}1-\nu & \nu & 0\\ \nu & 1-\nu & 0\\ 0 & 0 & (1-2\nu)/2\end{bmatrix} \tag{7}$$

When damage has not occurred, the relation $m=1/(2(1+\nu))$ holds, and matrix $[D']$ is identical to $[D]$. The proposed numerical analysis considered the strain-induced reduction of stiffness as well as strain softening effects of strength parameter, as indicated in Figs. 5 (a) and (b). This implies that the admissible space for stress is gradually shrunk as strain softening process takes place.

Any excess stress, which is computed on the transformed coordinate system based on slip plane direction and outside an updated failure envelope, is converted into unbalanced forces that are compensated for an iterative algorithm. Fig. 6 shows the modified stress by reduction of cohesion after yielding.

## 4. Studied Tunnel

### 4.1 Construction Site and Geology

The Rokunohe tunnel, 3,810 m long, is located at the northern end of the Honshu, between Hachinohe and Shin-Aomori in Japan (Kitagawa et al., 2005).

Fig. 7 showed the plan and vertical views of the construction site. In this Figure, Points A and B show the position of the studied tunnel. The tunnel section is located in Nos layer mainly as shown in Fig. 7. The geological profile of the ground consists of unconsolidated sand layer (Nos) in excess of 30m, which is lying beneath two layers of volcanic ash. Excavation of the bench was followed approximately 40m behind the face of the top heading excavation. Ahead of tunneling, deep wells are allocated along the tunnel route to lower the ground water level.

In addition, well point drainages at both sides of the upper bench are arranged to keep the floor dry. Fig. 8 shows the typical cross section of the tunnel.

Reinforcement of supports has been installed by using rockbolt, shotcrete and steel support. The tunnel will cross under the public facilities such as roads, railways, water channels for agriculture.

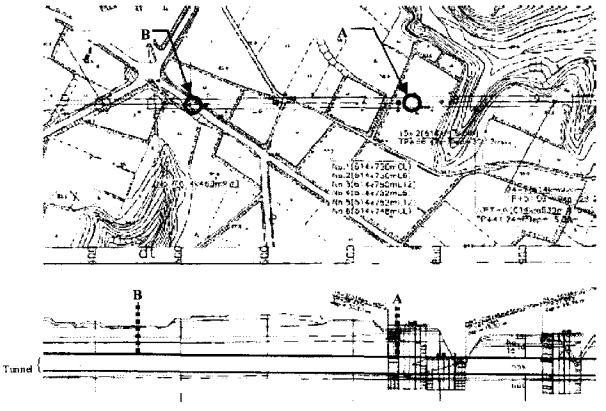


Fig. 7. Plan and vertical view of the site

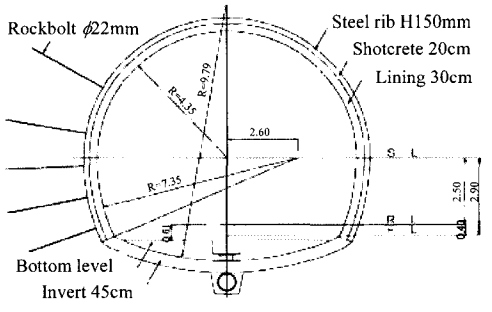


Fig. 8. Tunnel cross-section

### 4.2 Soil Test Result

Table 1 shows the soil properties of Nos layer. Fig. 9 shows the triaxial test result of this soil specimen sampled at 8m depth in studied tunnel area. In Fig. 9, it is shown by the relationships of axial stress ($\sigma_1$-$\sigma_3$)

Table 1. Soil properties of Nos layer

| | |
|---|---|
| Dry density | 2.6-2.8 g/cm$^3$ |
| Void ratio | 0.8-1.1 |
| Fine fraction content | 5-18% |
| Uniformity coefficient | 2.9 |
| Natural moisture content | 21-34% |
| Relative density | 100% over |
| N -value of SPT | 30-50 |

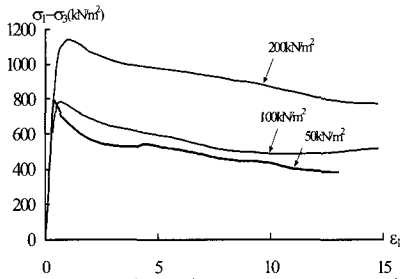


(a) Axial stress ($\sigma_1$-$\sigma_3$) versus axial strain ($\varepsilon_1$)

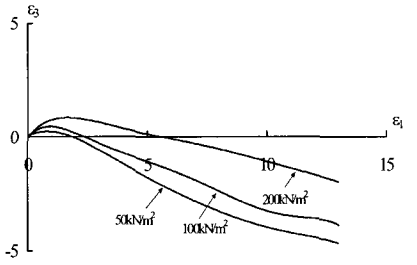


(b) Axial strain ($\varepsilon_1$) versus radial strain ($\varepsilon_3$)

Fig. 9. Triaxial compression test

versus axial strain ($\varepsilon_1$), and radial strain ($\varepsilon_3$) versus axial strain ($\varepsilon_1$). As shown in Fig. 9, soil behavior showed the softening effect after the peak strength. But, it is very difficult to define definitely the residual strength and incremental strain after passing the peak-point.

### 4.3 Measurement Method

In this tunnel project area, it was difficult to survey the level points using the manually-operated equipment owing to heavy snow cover of up to 1 m thick. Hence, the ground surface settlements were measured by means of auto tracking level together with leveling staves of a bar code type. Photo 1 shows the equipment to measure the ground surface settlement.

The auto tracking level autonomously collimates the leveling staves according to the preset directions at an interval of 30 minutes, and reads the bar code to measure the difference of elevation. Although this system does not have the function of three-dimensional measurement, this measuring method is economical when the vertical profiles are to be only measured. The degree of accuracy is 1mm at this range. Fig. 10 showed the plan of surface measurement around station 614 k 750 m. As shown in Fig. 10, six scan lines were set on the ground at 10 m interval and in total 78 leveling staves were installed to take the distribution of settlement. Because the auto tracking level itself settles down, it was necessary to compensate the measured values. Therefore, reference points were set at the location outside the area uninfluenced by the tunnel excavation. Fig. 11 shows the geological condition and measurement plan of two Sections, A and B.

In Section A, the thirteen leveling staves of a bar code type, three inclinometers, and two extensometers were installed to monitor the deformational behavior due to tunneling. And, the shear zone instrumentation with pipe gauge was performed for verification of the development

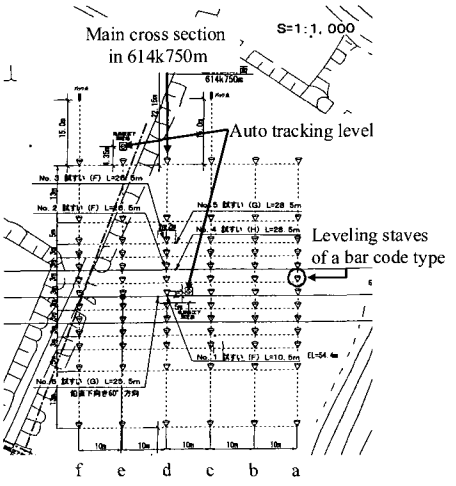


Fig. 10. Plan of surface measurement

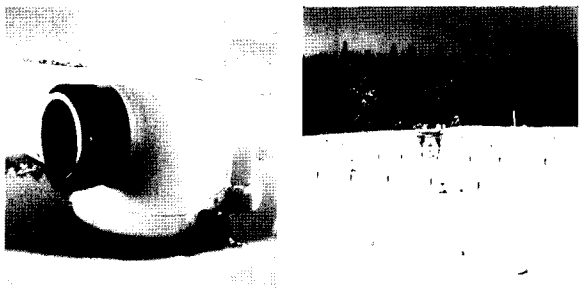

(a) Auto tracking level (b) Measurement area

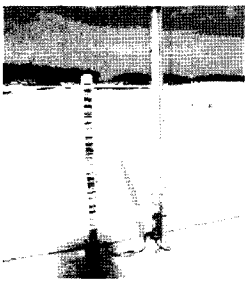

(c) Leveling staves of a bar code type

Photo 1. Equipments for measurement

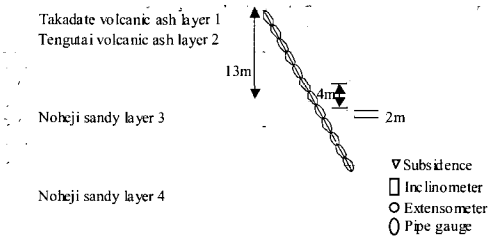


(a) Section A

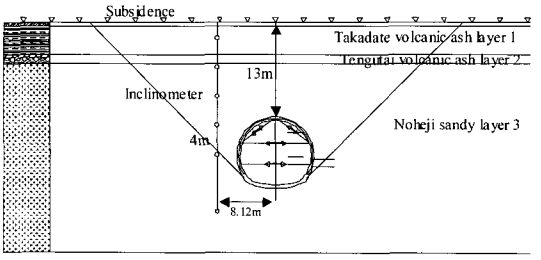


(b) Section B

Fig. 11. Measurement plan

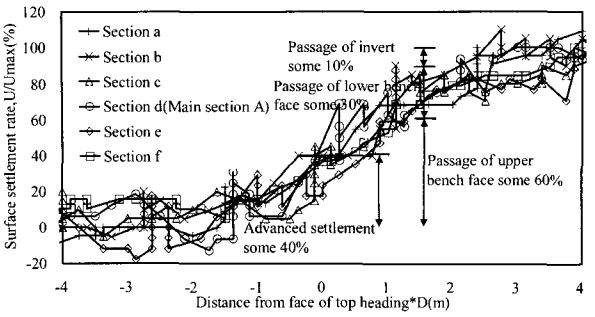


Fig. 12. Maximum surface settlement with main Section A and near 5 sections

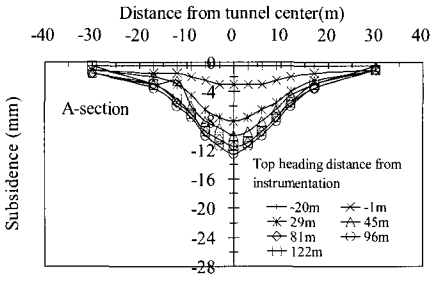


(a) Subsidence

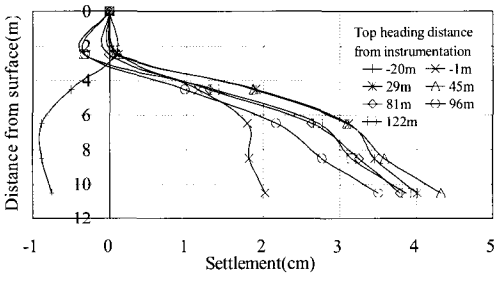


(b) Extensometer above tunnel

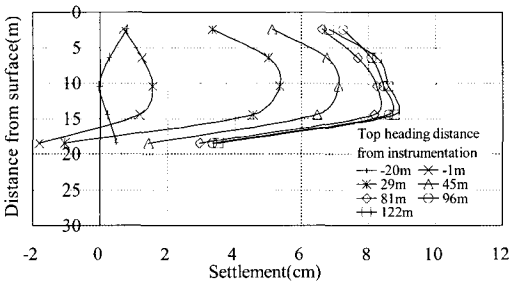


(c) Extensometer at 6 m from centerline

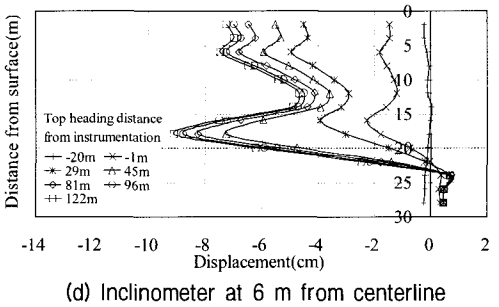


(d) Inclinometer at 6 m from centerline

Fig. 13. Measurement results in Section A

of shear band from tunnel side. This gauge is set up 30 m length by $60^0$ from the surface plan. In Section B, the nineteen leveling staves of a bar code type and one extensometer were installed to monitor the deformation behavior.

## 4.4 Measurement Results

### 4.4.1 Section A

Fig. 12 shows the ratio of ground surface settlement to maximum settlement right above the tunnel center with the distance from the face of the top heading.

The maximum settlement was approximately 12mm. The settlement began when the face of the top heading reached the 12 m (1.5D) ahead of the measuring section. The fractions of the total settlement at each stage of excavation were 60% (upper half section), 30% (lower half section), and 10% (invert). The advanced settlement was 40% of the total one. Fig. 13 shows subsidence, subsurface settlement and the horizontal displacement due to tunneling in Section A. Fig. 14 shows the bending deformation that is estimated from the measurement of the pipe strain meters. In this figure, it appears that the mode of deformation with growing the shear bands forms at tunnel side.

Though the magnitude of deformation is small, the bending mode of the pipe suggests that the shear band formation was already in progress to some extent. This is not an easy phenomenon to identify from standard pattern of the displacement monitoring, but definitely it is very important behavior that should not be missed.

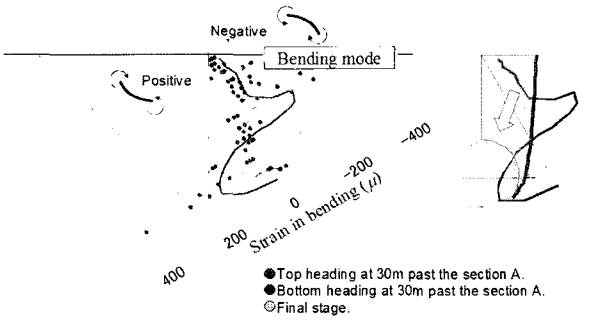


Fig. 14. Bending of pipe gauge embedded in Section A

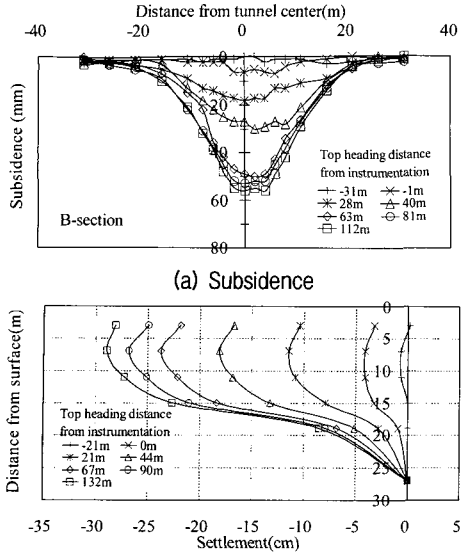


Fig. 15. Measurement results in Section B

### 4.4.2 Section B

Fig. 15 shows surface settlement and subsurface settlement due to tunneling in Section B.

The maximum subsidence was measured to be more than 50 mm. The magnitude of the maximum settlement observed for this section was approximately 60 mm which is about 5 times bigger than that of Section A (nearly 12 mm). In two cross sections, it is considered that the different mode of deformation happened although ground condition and tunnel geometry are similar.

## 5. Numerical Simulation in Studied Tunnel

### 5.1 Outline of Numerical Analysis

Numerical simulations were conducted for two cross sections with slightly different geometric configuration. Geometry and boundary conditions of the finite element meshes are shown in Fig. 16.

Due to symmetry in the geometry, only the right half of the tunnel has been analyzed. In the analysis boundary domain has an extent of some 3 time (downward) and 4 time (sideward) of tunnel diameter from tunnel axis. Both sides of the mesh are horizontally fixed axis and the bottom nodes are vertically fixed. The ground behavior was modeled with three different constitutive laws;

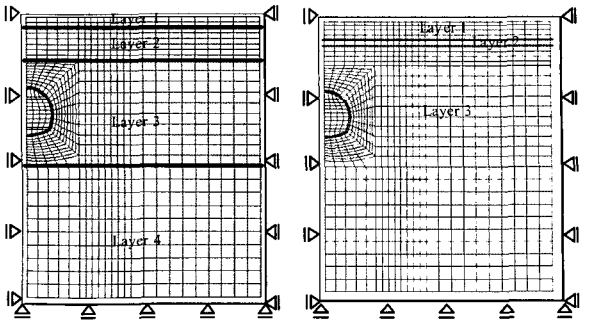


Fig. 16. Finite element mesh

namely 1) an elastic model, 2) elastic-plastic material model with a Mohr-Coulomb failure criterion and 3) the strain softening model proposed in this paper. Shotcrete and steel support were modeled as elastic elements. Simulation has been performed in several computational steps for excavation of the tunnel top heading in advance followed by bench (lower section) and invert excavation. The finite element simulation of the tunnel excavation through soils should ideally be performed by using the 3D analysis that is typically not performed for most projects. Thus, the methodology that approximately accounts for 3D effects by using the 2D analysis was employed.

Panet and Guenot (1982) showed how the three dimensional problem due to the presence of the tunnel face can be reduced to an equivalent plane strain problem by using stress release factor. This paper selected the stress release factor of 40%/60% considering the rate of maximum surface settlement. In Fig. 11 40% stress release ratio with excavation of the top heading (upper section) has been applied and the support has been put in place and, at the same time, the remaining 60% of the excavation forces has been released. The horizontal stress ratio, $K_0$, is calculated by $\nu/(1-\nu)$, where $\nu$ is Poisson's ratio. Tables 2 and 3 showed the material properties and support member's value used FEM simulation. Numerical simulation, firstly, is carried out with material property values, $E$, $\nu$, $c$, and $\phi$, obtained from laboratory and field tests. Strain softening parameters are difficult to determine by laboratory test. However, as for strain softening analysis, parametric study was performed in which $\Delta\gamma$

and β was varied resulting in the total of 9 cases as shown in Table 4. The results of numerical analysis showed that, in initial construction stages, the measured ones are smaller than the predicted values in design stages. Secondly, on construction, a series of parameter tunings are performed for better agreement between computed and measured quantities at the top heading excavation before the bench excavation. The identified parameters at top heading excavation were then used to predict displacements at the final excavation stage.

## 5.2 Results of Numerical Simulation

### 5.2.1 Prediction of Ground Displacement

Fig. 17 showed surface subsidence and gradient from 3 different material models and the measurement defined for the final stage.

Fig. 18 showed the comparison between measured and calculated ground displacement by extensometer and inclinometer. Figs. 17 and 18 show that softening analysis is in good agreement with the result of the field data. As for the results of strain softening analysis, the one that

Table 2. Material parameters used FEM at Sections A and B

| Section A | | | | |
|---|---|---|---|---|
| Material properties | Layer 1 | Layer 2 | Layer 3 | Layer 4 |
| | Takadate volcanic ash | Takadate volcanic ash | Noheji sandy | Noheji sandy |
| $r(kN/m^3)$ | 14 | 18 | 20 | 20 |
| $E$ (MPa) | 10 | 10 | 160 | 200 |
| $v$ | 0.286 | 0.286 | 0.286 | 0.286 |
| $\phi(0)$ | 0 | 0 | 35 | 35 |
| $c$ (MPa) | 30 | 45 | 30 | 50 |
| Ratio of strength parameter, $\beta_c$, $\phi_{(0)}$(%) | 50 | 50 | 50 | 50 |
| Strain incremental ratio, $\Delta\gamma$ | 0.01 | 0.01 | 0.01 | 0.01 |
| Ratio of anisotropy reduction $\beta m$(%) | 50 | 50 | 50 | 50 |
| Horizontal stress ratio, $K_0$ | 0.98 | | | |
| Section B | | | | |
| Material properties | Layer 1 | | Layer 2 | Layer 3 |
| | *Takadate volcanic ash* | | *Tengutai volcanic ash* | *Noheji sandy* |
| $r(kN/m^3)$ | 14 | | 18 | 20 |
| $E$ (MPa) | 8 | | 8 | 128 |
| $v$ | 0.286 | | 0.286 | 0.286 |
| $\phi(0)$ | 30 | | 45 | 30 |
| $c$ (MPa) | 0 | | 0 | 35 |
| Ratio of strength parameter, $\beta_c$, $\phi_{(0)}$(%) | 35 | | 35 | 35 |
| Strain incremental ratio, $\Delta\gamma$ | 0.01 | | 0.01 | 0.01 |
| Ratio of anisotropy reduction $\beta m$(%) | 35 | | 35 | 35 |
| Horizontal stress ratio, $K_0$ | 0.7 | | | |

Table 3. Support members used FEM

| | | |
|---|---|---|
| Supoport parameter (Plane element; shotcrete and steel support) | Initial support, E(MN/m$^2$) | 5000 |

Table 4. 9 Case for strain softening analysis

| Softening parameter pattern | | Residual 80% | strength/Original 60% | Strength, β 40% |
|---|---|---|---|---|
| $\Delta\gamma$ | 0.04 | Case 1 | Case 4 | Case 7 |
| | 0.02 | Case 2 | Case 5 | Case 8 |
| | 0.01 | Case 3 | Case 6 | Case 9 |

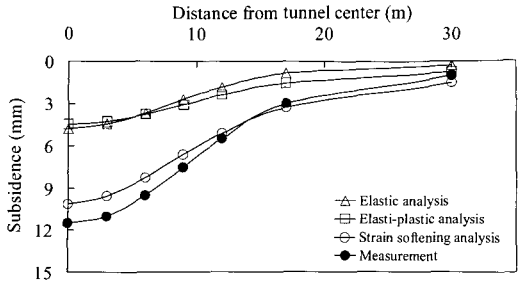


(a) Subsidence of Section A

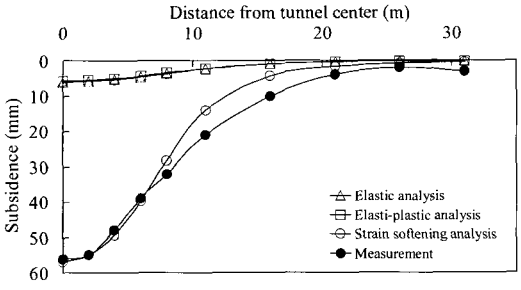


(b) Subsidence of Section B

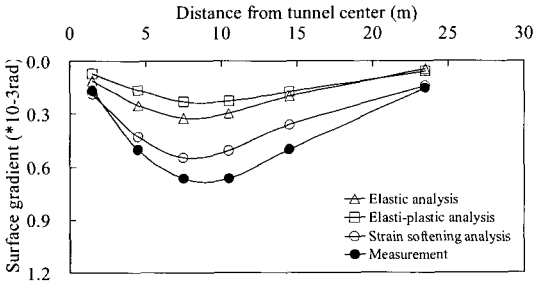


(c) Surface gradient of Section A

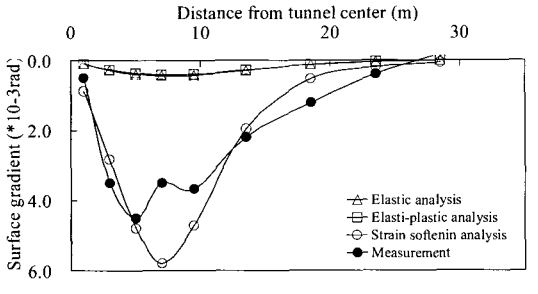


(d) Surface gradient of Section B

Fig. 17. Comparison between measured and calculated subsidence and gradient

gave the closest results to the measurement is shown for both cross sections. For Section A, where the maximum subsidence was around 10 mm, the results from different models show insignificant differences. On the contrary, for Section B, the displacement in excess of 50 mm was measured; the superiority of the softening model is seen

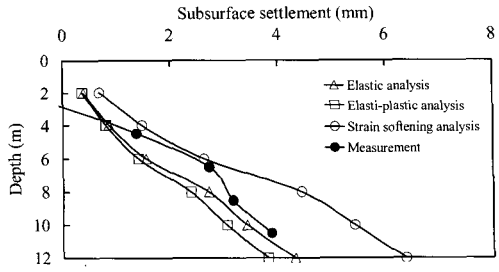


(a) Extensometer above tunnel in Section A

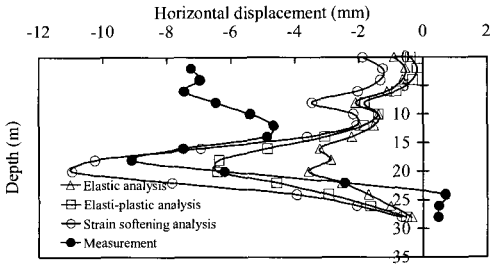


(b) Inclinometer at near side in Section A

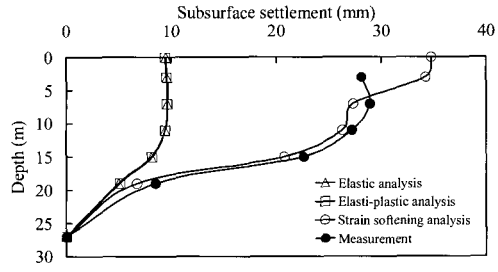


(c) Extensometer at near side in Section B

Fig. 18. Comparison between measured and calculated ground displacement

as compared to elastic or elasto-plastic analysis. A clear advantage of the strain softening analysis is seen here for Section B, where the shear band development might have occurred to produce this particular profile of surface subsidence.

### 5.2.2 Development of Maximum Shear Strain Distribution

Fig. 19 shows the maximum shear strain distribution at the final stage of analysis for two sections. It is seen that for Section A, all material models showed similar images since the magnitude of displacement was constrained to fairly low level.

However, for Section B, the case which showed the best results in comparison with the measurement, namely the result from the softening analysis, shows the development of shear band from tunnel shoulder. The

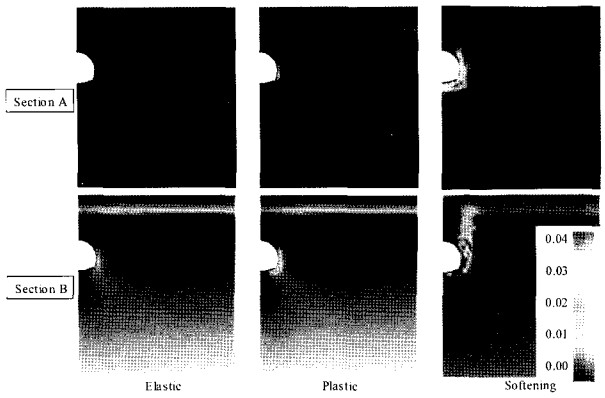


Fig. 19. Maximum shear strain distribution

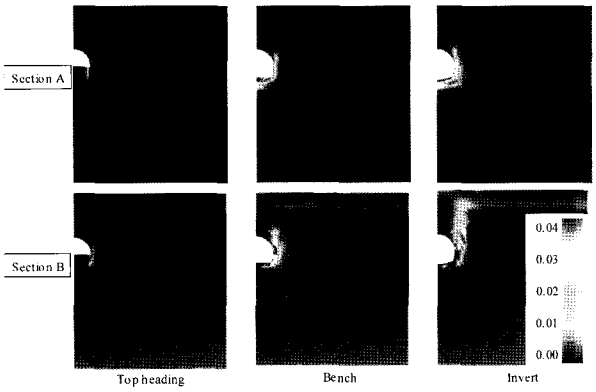


Fig. 20. Maximum shear strain distribution in the strain softening analysis

band is believed to be of the fair size, although it has not reached the surface of the ground. However, this development of the shear band is regarded as the cause of the large displacement that occurred for this section. Fig. 20 showed the development of maximum shear strain distribution due to the excavation stage in strain softening modeling. In Section B, it is known that shear band developed at the bench excavation.

## 6. Conclusion

In urban area, tunnel construction is usually important in terms of prediction and control of surface settlement and gradient. This paper has studied the application of new computational modeling to predict and identify deformation behavior around ground of urban NATM tunnel.

The proposed numerical procedure considered the reduction of shear stiffness and strength parameter after yielding with strain softening effects of a given material. The numerical analysis results produced a strain distribution, deformational mechanism and surface settlement profile, which are in good agreement with the results of case study. The proposed numerical approach will be a good prediction method on the ground displacement associated with NATM tunneling in shallow depth and soft ground.

## Acknowledgments

This research was conducted under the Technical Committee of Tohuku Shin-Kansen Tunnel organized by the Japan Railway Construction, Transport and Technology Agency. Also, technical contribution from Mr T. Kitagawa, Mr A. Isogai, Mr K. Yashiro of Japan Railway Research Institute, Mr T. Sudo of Taisei Corporation, Mr T. Matsunaga of Pacific consultants, Mr N. Doba of Kajima Corporation are greatly appreciated. This work was supported by the Brain Korea 21 Project in 2007.

## References

1. Adachi, T., Tamura, T., Yashima, A. and Ueno, H. (1985), Behavior and simulation of sandy ground tunnel, *Proceedings of JSCE*, No.358, III-3, pp.129-136.
2. Akutagawa, S., Kitani, T. ,Matsumoto, K. and Mizoguchi, S. (2001), Numerical modeling of a nonlinear deformational behavior of a tunnel with shallow depth, *Modern Tunneling Science and Technology. (IS -Kyoto)*, Adachi et al eds, pp.111-114.
3. Akutagawa, S., Otazawa, H. and Sakurai, S. (2006), Numerical simulation of a large scale slope failure considering reduction of stiffness and strength over time, *Journal of the Society of Materials Science*, Japan, Vol.55, No.5, pp.515-522.
4. Gioda, G. and Locatelli, L. (1999), Back analysis of the measurements performed during the excavation of a shallow tunnel in sand, *International Journal for Numerical and Analytical Methods in Geomechanics*, Vol.23, pp.1407-1425.
5. Hansmire, W. H. and Cording, E. J. (1985), Soil tunnel test section; Case history summary, *Journal of Geotechnical Engineering*, ASCE, Vol.111, No.11, pp.1301-1320.
6. Kitagawa, T., Iida, H., Sudo, T., Matsunaga, T., Akutagawa, S., and Konishi, S. (2005), Tunneling and measurements in unconsolidated ground, *Proceedings of the 31st ITA-AITES WORLD TUNNEL CONGRESS*, Underground Space Use: Analysis of the Past and Lessons for the Future, Erdem & Solak(eds.), Turkey, pp.897-902.
7. Matsumoto, K. (2000), Fundamental investigation of design pressure of tunnels, Masters thesis, Graduate School of Science and

Technology, *Kobe University*, Japan.

8. Matsunaga, T., Kitani, T., Konishi, S., Akutagawa, S. and Murakami, K. (2002), Applicability of the strain softening model for the research of the surface settlement, *37th Pro. of JSCE*, pp.1677-1678.
9. Murayama, S. and Matsuoka, H. (1969), On the settlement of granular media caused by the local yielding in the media, *Proceedings of JSCE*, Vol.172, pp.31-41.
10. Negro, A. and de Queiroz, P. I. B. (2000), Prediction and performance: A review of numerical analyses for tunnels, *Geotechnical Aspects of Underground Construction in Soft Ground*, edited by Fujita and Miyazaki, pp.409-418.
11. Okuda, M., Abe, T. and Sakurai, S. (1999), Nonlinear analysis of a shallow tunnel, *Journal of Geotechnical Engineering*, JSCE, 638(III-49): pp.383-388.
12. Panet, M. and Guenot, A. (1982), Analysis of convergence behind the face of a tunnel, *Tunneling '82*, London, pp.197-204.
13. Sakurai, S and Akayuli, C.F.A. (1998), Deformational analysis of geomaterials considering strain-induced damage, In;Cividini, A.(ed), *Proc. 4th*. Europ., pp.729-738.
14. Shahin, H. M., Nakai, T., Hinokia, M. and Yamaguchi, D. (2004), 3D effect of earth pressure and displacements during tunnel excavations, *Soils and foundations*, Japanese Geotechnical Society, Vol.44, No.5, pp.37-49.
15. Sterpi, D. (1999), An analysis of geotechnical problems involving strain softening effects, *Int. J.Num. Analyt. Meth. Geomech.*, 23, pp.1427-1454.
16. Wong, R. C. K. and Kaiser, P. K. (1987), Prediction of ground movements above shallow tunnels, Prediction and Performance in Geotechnical Engineering, *Calgary*, June, pp.329-343.

(received on Jul. 2, 2007, accepted on Sep. 26, 2007)